

Supporting Information

Hierarchical 2D Yarn-ball Like Metal-Organic Framework NiFe(dobpdc) as Bifunctional Electrocatalyst for Efficient Overall Electrocatalytic Water Splitting

Lixia Qi,^{a‡} Ya-Qiong Su,^{b‡} Zichen Xu,^a Guanghui Zhang,^c Kang Liu,^d Min Liu,^d Emiel J.M.

Hensen,^b and Ryan Yeh-Yung Lin^{*a}

^aState Key Laboratory of Fine Chemicals, Zhang Dayu School of Chemistry, Dalian University of Technology, Dalian 116024, P. R. China

^bLaboratory of Inorganic Materials and Catalysis, Department of Chemical Engineering and Chemistry, Eindhoven University of Technology, P.O. Box 513, 5600 MB, Eindhoven, The Netherlands

^cState Key Laboratory of Fine Chemicals, PSU-DUT Joint Center for Energy Research, School of Chemical Engineering, Dalian University of Technology, Dalian 116024, P. R. China

^dSchool of Physics and Electronics, State Key Laboratory of Powder Metallurgy, Central South University, Changsha 410083, Hunan, P. R. China

[‡]These authors contributed equally.

*Corresponding Author. E-mail: yylin@dlut.edu.cn

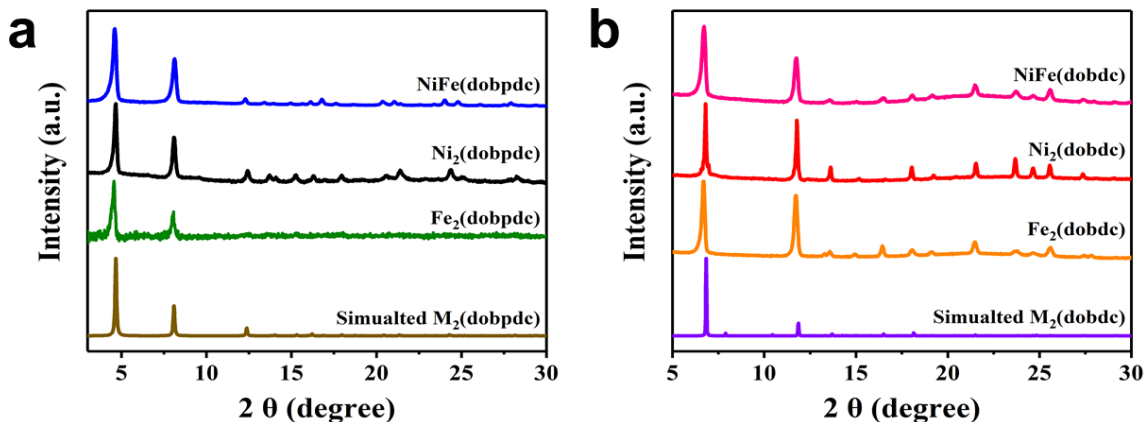


Fig. S1 The PXRD patterns of (a) M₂(dobpdc) and (b) M₂(dobdc) series MOFs.

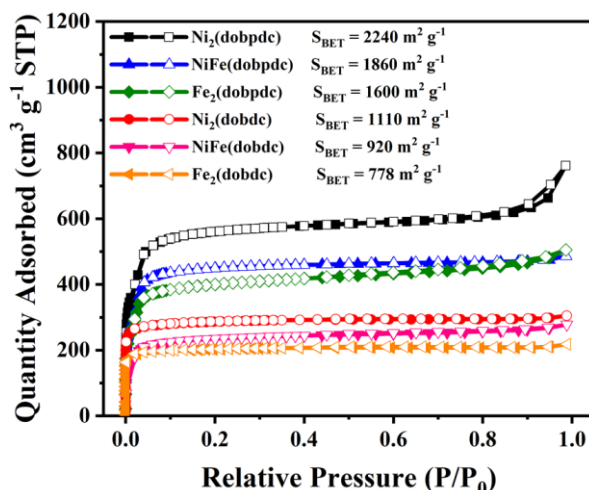


Fig. S2 The N₂ isothermal absorption-desorption curves of MOFs at 77K.

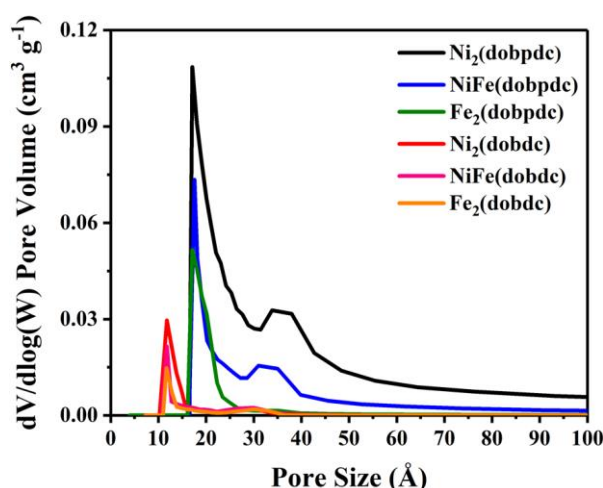


Fig. S3 Pore size distribution of MOFs.

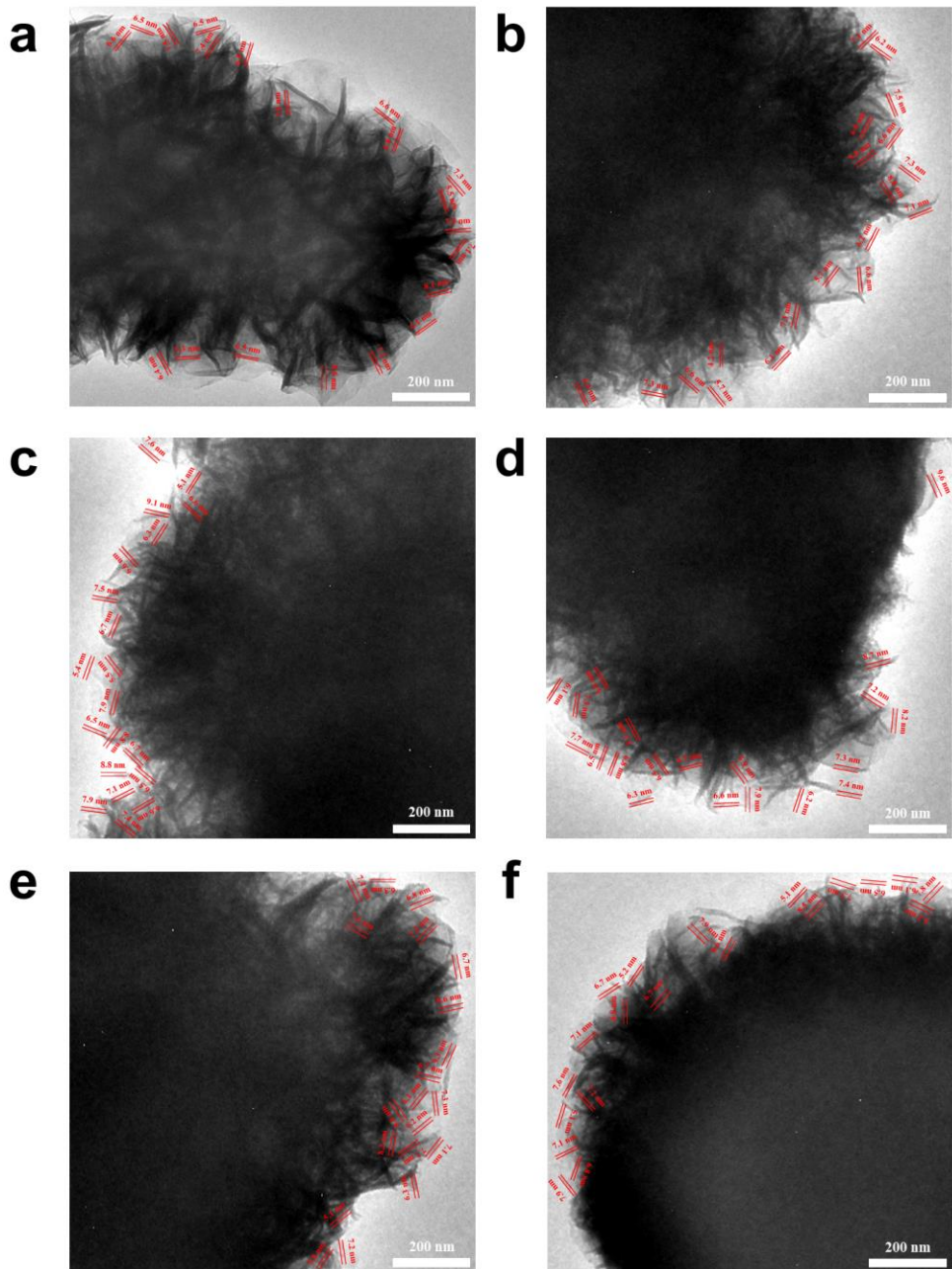


Fig. S4 TEM images for calculation the thickness distribution of NiFe(dobpdc).

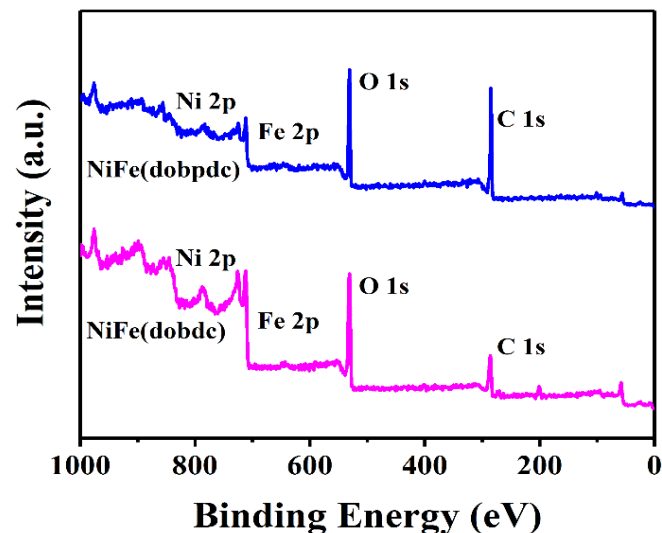


Fig. S5 Full range XPS survey spectra of NiFe(dobpdc) and NiFe(dobdc), respectively.

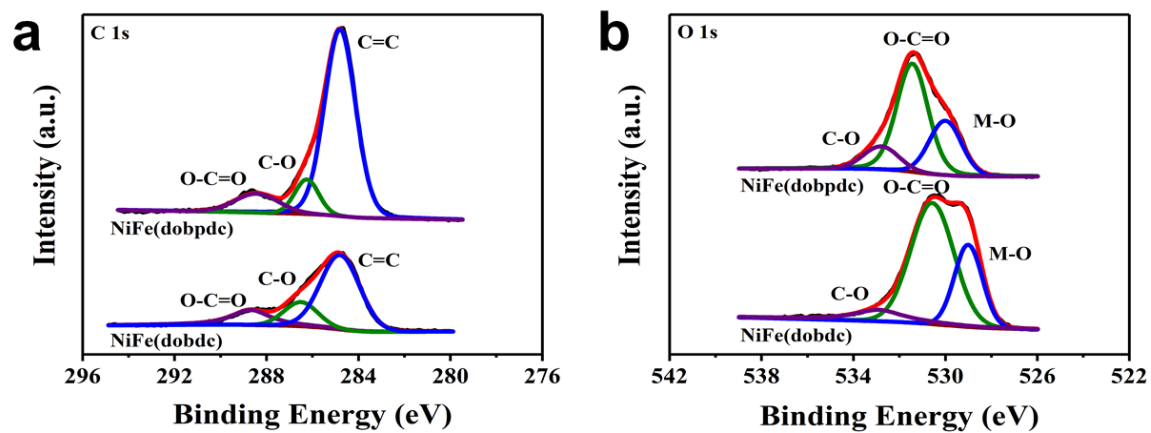


Fig. S6 High-resolution XPS spectra of NiFe(dobpdc) and NiFe(dobdc). (a) C 1s spectra and (b) O 1s spectra.

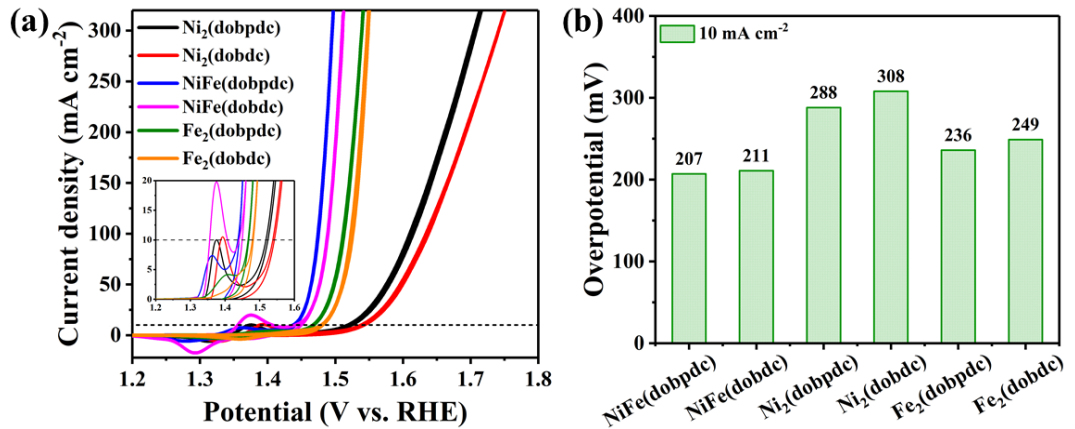


Fig. S7 (a) CV curves of MOF electrocatalysts for OER. (b) overpotentials required for OER at $j = 10$.

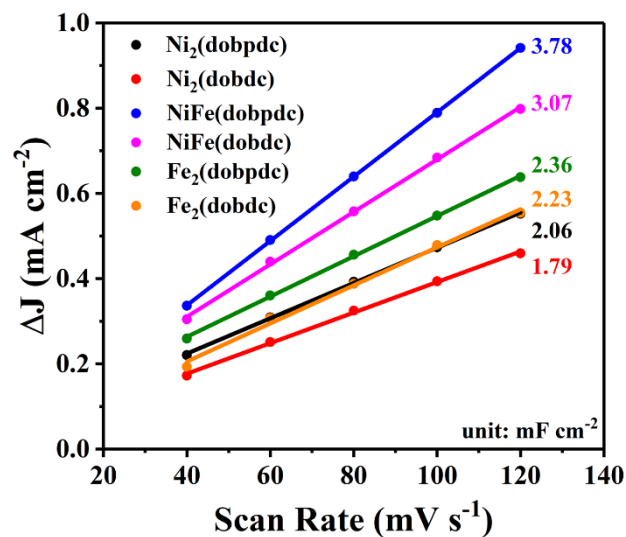


Fig. S8 C_{dl} calculations at 1.05 V vs RHE of MOF electrocatalysts.

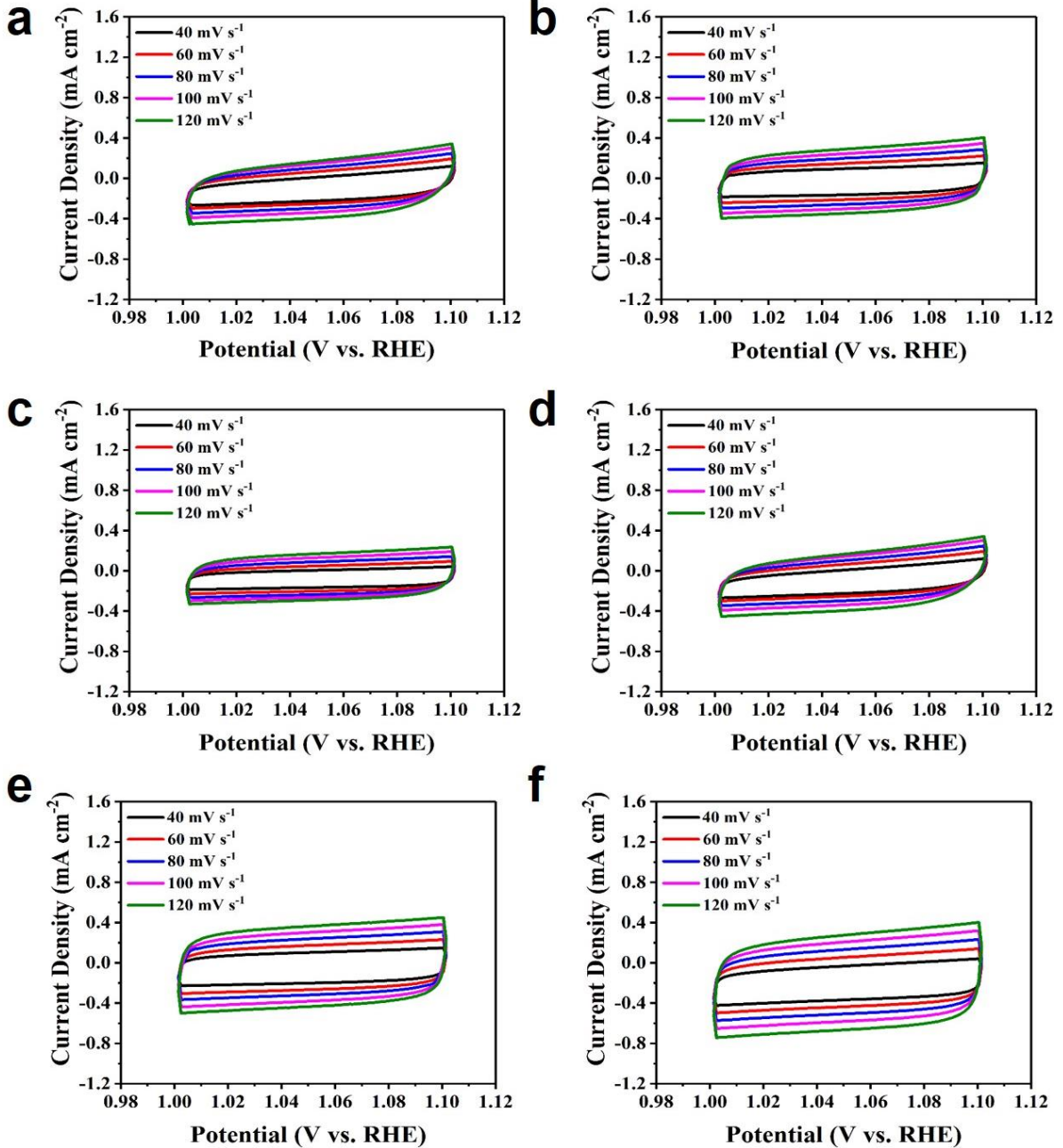


Fig. S9 CV curves between 1.0 and 1.1 V vs RHE for (a) Fe₂(dobdc), (b) Fe₂(dobpdc), (c) Ni₂(dobdc), (d) Ni₂(dobpdc), (e) NiFe(dobdc) and (f) NiFe(dobpdc).

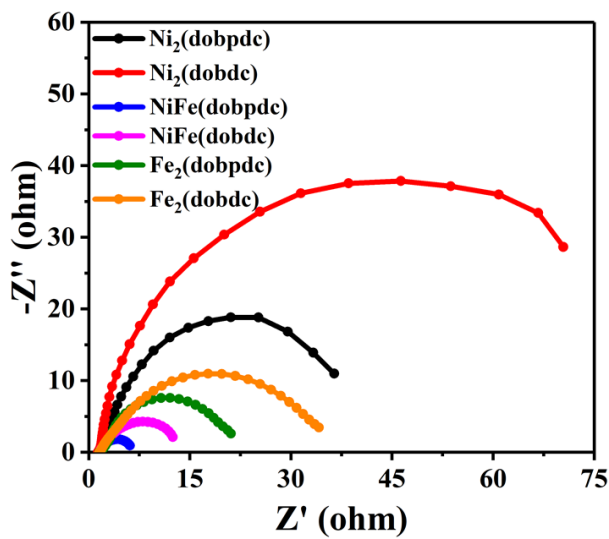


Fig. S10 Nyquist plots recorded of MOF electrocatalysts for OER.

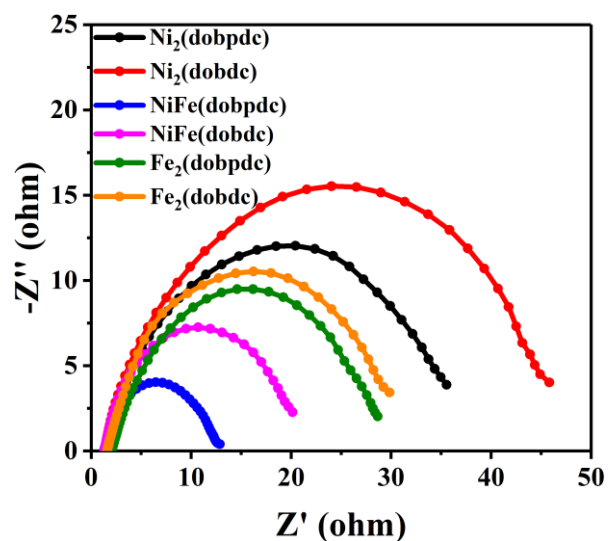


Fig. S11 Nyquist plots recorded of MOF electrocatalysts for HER.

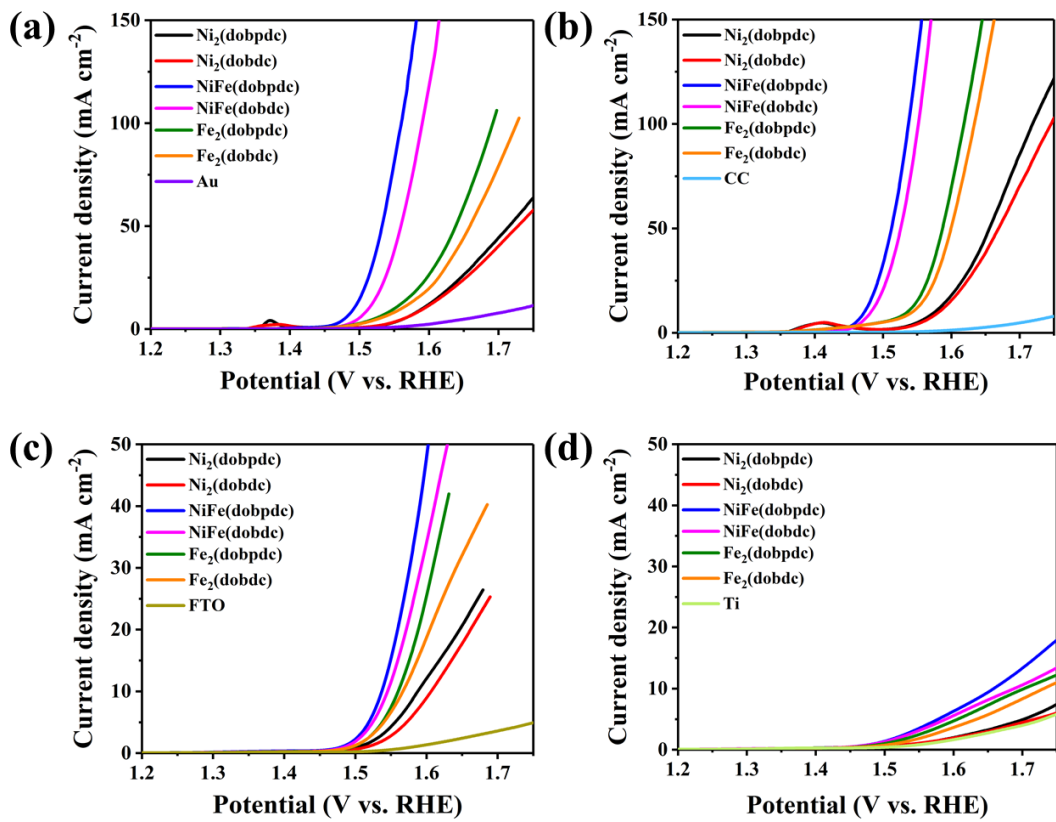


Fig. S12 OER performance of MOF electrocatalysts on the substrates of (a) Au plate, (b) carbon cloth, (c) FTO and (d) Ti foam, respectively.

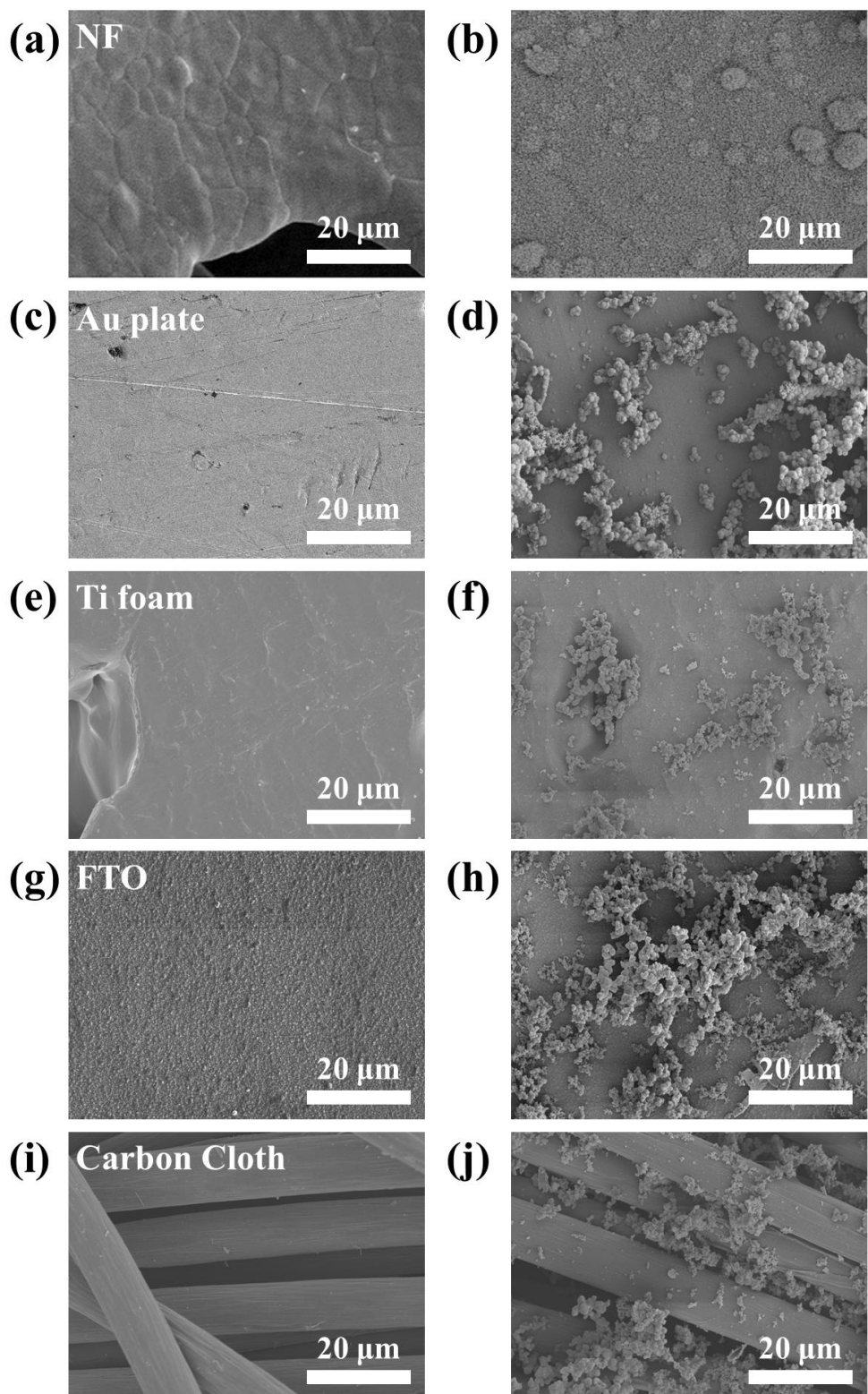


Fig. S13 SEM images of bare (a) NF, (c) Au plate, (e) Ti foam, (g) FTO and (i) carbon cloth, respectively. SEM images of NiFe(dobpdc) growth on (b) NF, (d) Au plate, (f) Ti foam, (h) FTO and (j) carbon cloth, respectively.

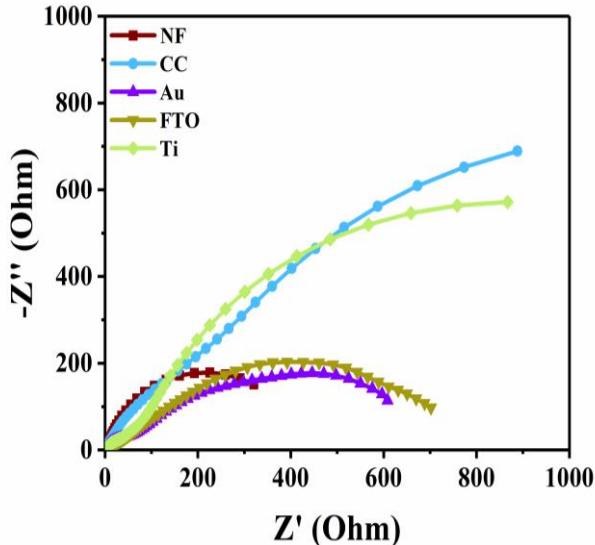


Fig. S14 Nyquist plots recorded of bare NF, Au plate, Ti foam, FTO and carbon cloth for OER.

Discussion the activity of Fe₂(dobpdc) and influence of nickel foam substrate:

The OER activity of MOF electrocatalysts on four different substrates, namely, Au plate, Ti foam, FTO glass and carbon cloth are showed in Fig. S12†. Based on the LSV results, the OER activity of the MOF electrocatalysts on the abovementioned substrates is consistent with that on NF. As expected, the NiFe-MOFs have the best OER performance. Notably, Fe-based MOFs with OER activity are better than Ni-based MOFs on all four substrates. These results indicate that compared with Ni-based MOFs, Fe-based MOFs have intrinsically better electrocatalytic activity. Besides, Fe₂(dobpdc) has a much higher electrical conductivity than Ni₂(dobdc).^{1,2} On the other hand, the SEM images (Fig. S13b†) showed that the *in situ* growth of NiFe(dobpdc) on NF is dense; in contrast, NiFe(dobpdc) shows sparse and rare growth on flat substrates, namely, the Au plate, Ti foam, FTO glass and fiber structure of carbon cloth (Fig. S13d, f, h and j†). This result can be attributed to NF being a 3D-framework material that benefits MOF growth compared to other substrates. In addition, NF shows a lower EIS (Fig. S14†) for the OER, indicating that NF has good conductivity, benefiting charge transport. These results explain why MOFs on NF have much better electrocatalytic performance for the OER than other substrates. Therefore, the high catalytic activity for the OER of Fe₂(dobpdc) and Fe₂(dobdc) on the NF substrate is mainly attributed to their high electrical conductivities and intrinsic electrocatalytic activities.

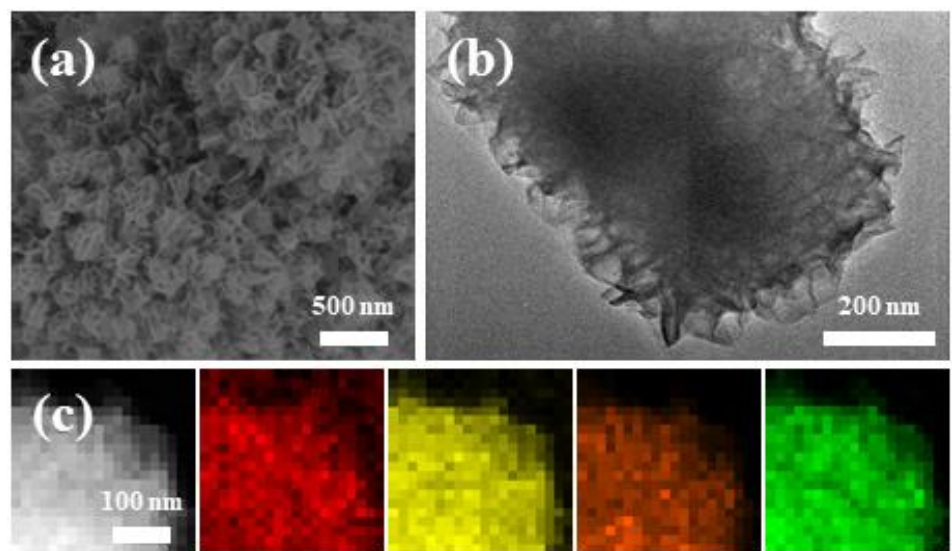


Fig. S15 (a) SEM, (b) TEM and (c) TEM-EDS mapping images of NiFe(dobpdc) after long-term electrocatalytic OER. The red, yellow, orange, and green represents the carbon, oxygen, iron and nickel atoms, respectively.

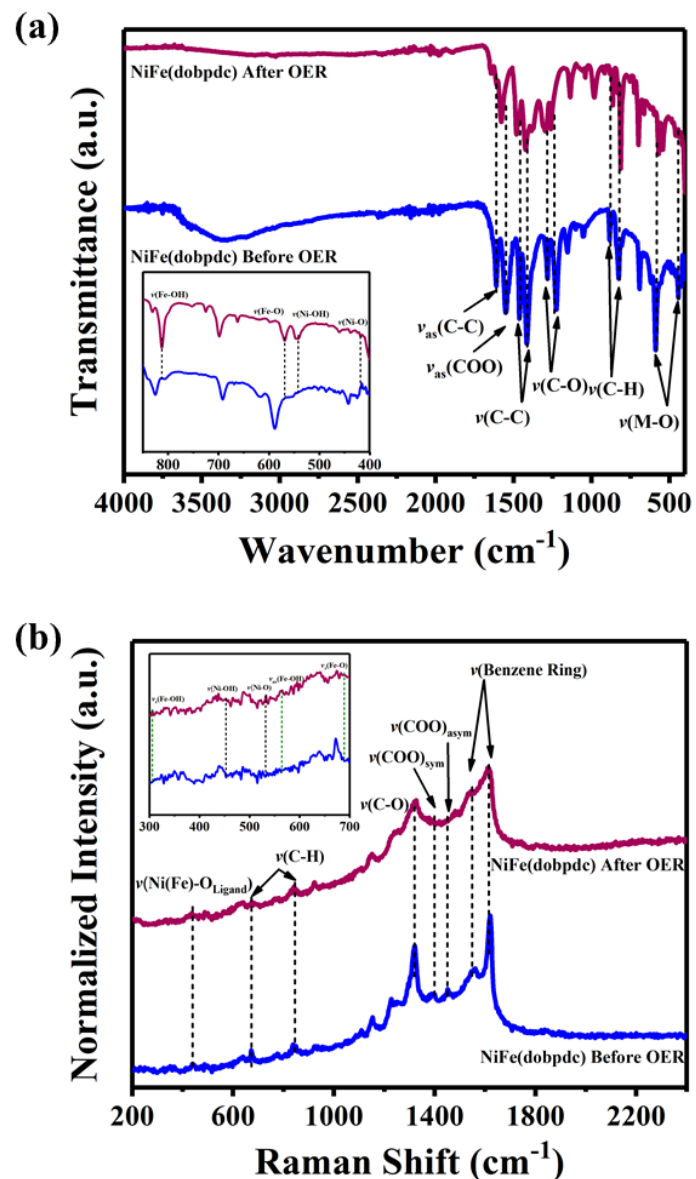


Fig. S16 (a) FTIR and (b) Raman spectra of NiFe(dobpdc) before and after long-term electrocatalytic OER.

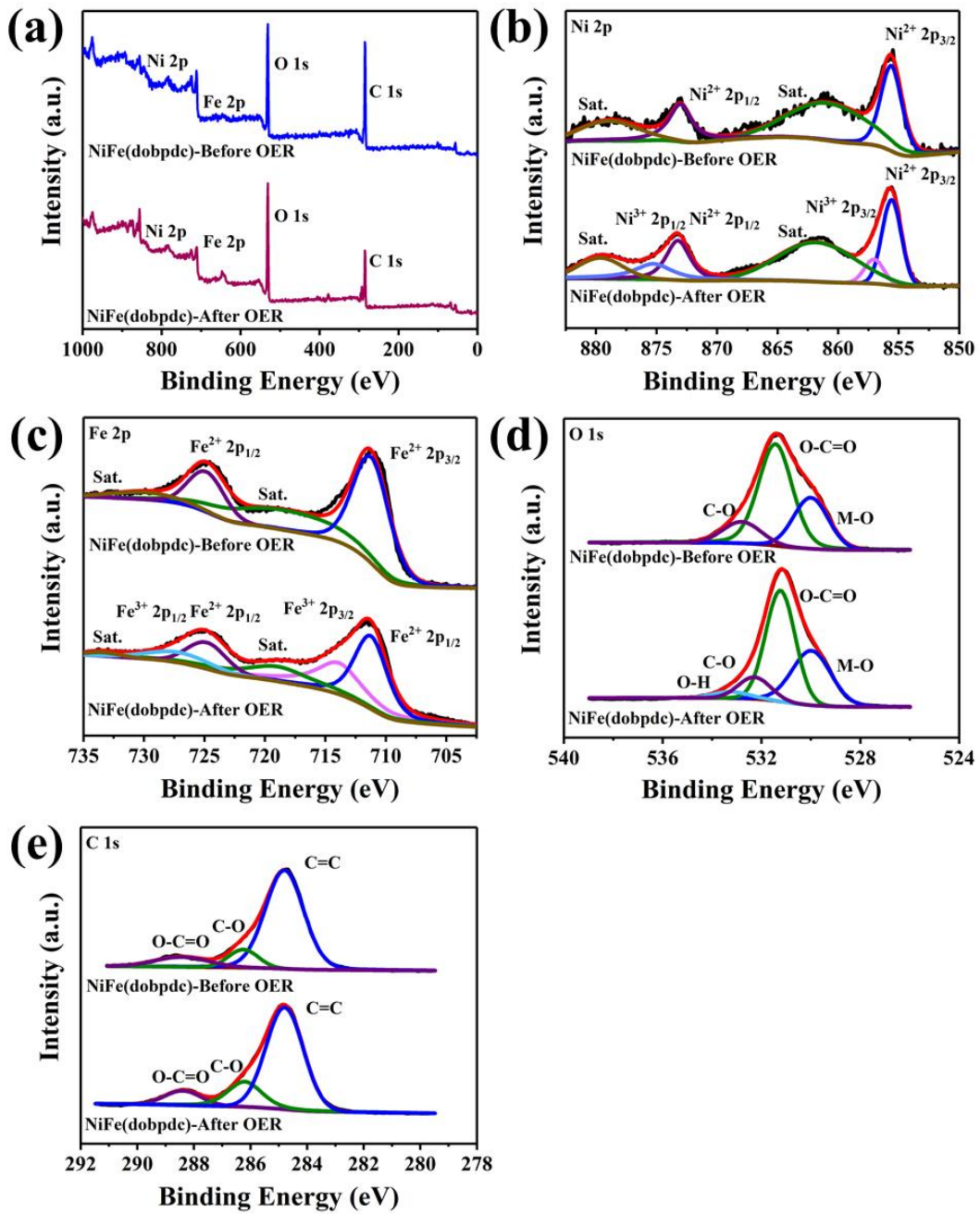


Fig. S17 High-resolution XPS spectra of NiFe(dobpdc) before and after long-term electrocatalytic OER. (a) full range XPS survey spectra (b) Ni 2p, (c) Fe 2p, (d) O 1s and (e) C 1s.

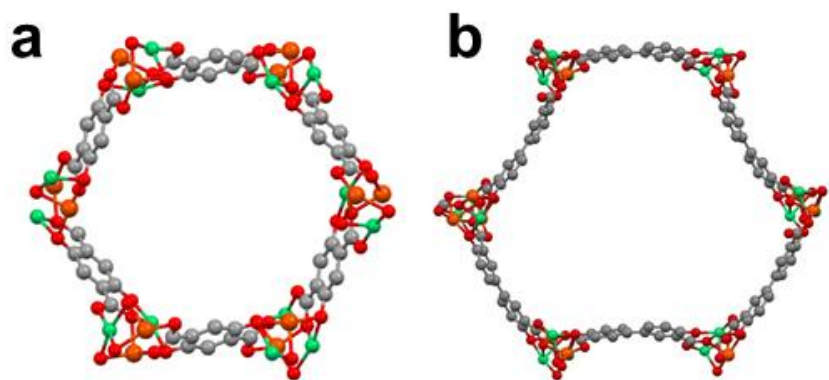


Fig. S18 The DFT calculated modes of (a) NiFe(dobdc) and (b) NiFe(dobpdc). The green, orange, red and gray represents the nickel, iron, oxygen and carbon atoms, respectively.

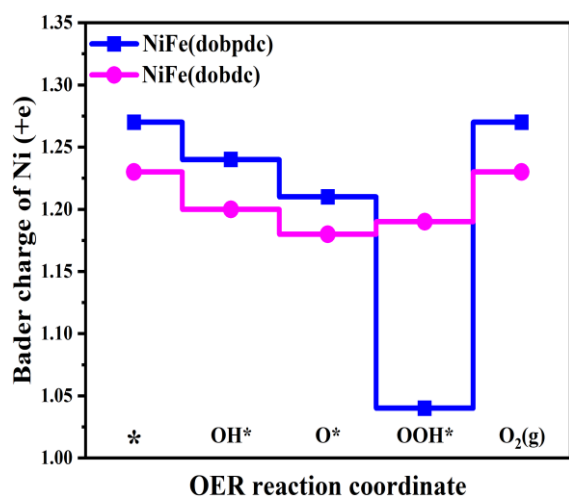


Fig. S19 Bader charge analysis of Ni sites in NiFe(dobdc) and NiFe(dobpdc) during OER process.

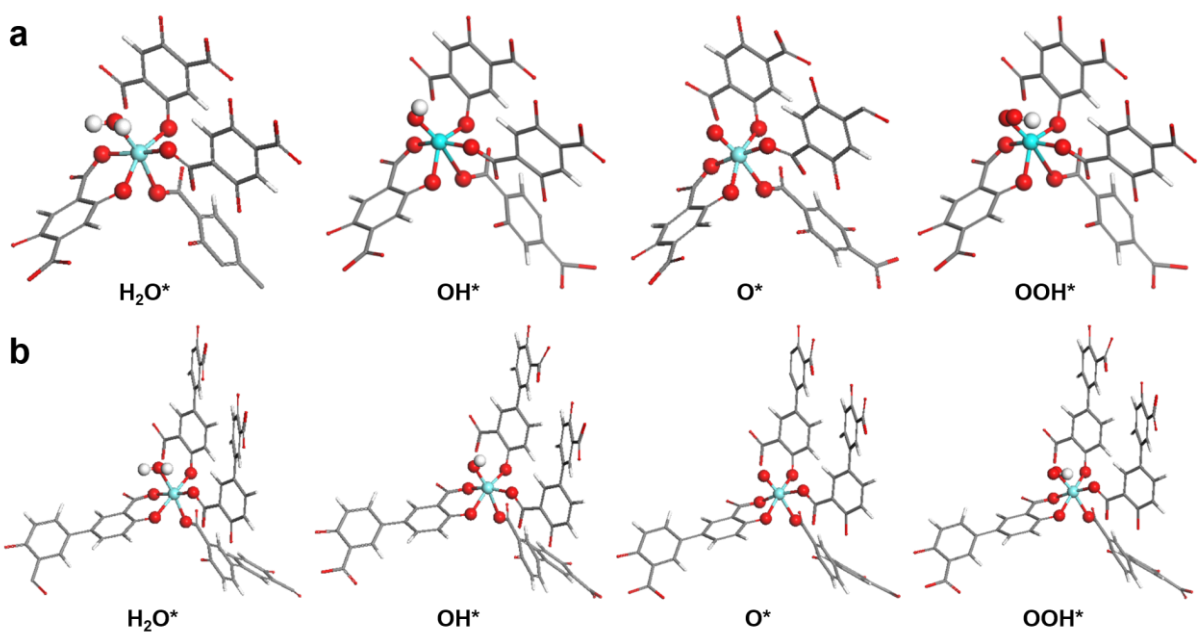


Fig. S20 The optimized structures of different adsorption intermediates for (a) NiFe(dobdc) and (b) NiFe(dobpdc), respectively. The cyan, red and white balls are the activity metal center, oxygen and hydrogen, respectively.

Table S1 EXAFS fitting parameters of Ni *R*-space for NiFe(dobpdc) and NiFe(dobdc), respectively.

MOF	Shell	C.N.	σ^2 (10 ⁻³ Å ²)	R (Å)
NiFe(dobdc)	Ni-O	6.1	5	2.02
NiFe(dobpdc)	Ni-O	6.2	8	2.01

Table S2 EXAFS fitting parameters of Fe *R*-space for NiFe(dobpdc) and NiFe(dobdc), respectively.

MOF	Shell	C.N.	σ^2 (10 ⁻³ Å ²)	R (Å)
NiFe(dobdc)	Fe-O	4.8	7	2.01
NiFe(dobpdc)	Fe-O	5.2	8	1.99

Table S3 Electrocatalytic OER and HER performance of the NiFe-based MOF and relevant electrocatalysts.

Catalysts	Electrolyte	OER		HER		Reference
		η (mV @ mA cm ⁻²)	Tafel slopes (mV dec ⁻¹)	η (mV @ mA cm ⁻²)	Tafel slopes (mV dec ⁻¹)	
NiFe(dobpdc)	1.0 M KOH	207 @ 10 251 @ 100	36	113 @ 10 170 @ 100	69	This work
Fe-Ni@NC-CNTs	1.0 M KOH	274 @ 10	45.47	202 @ 10	113.7	3
FeNi(BDC)(DMF,F)/NF (Fe:Ni=5:1)	1.0 M KOH	227 @ 60	37.4	160 @ 10	96.2	4
NFN-MOF/NF	1.0 M KOH	240 @ 10	58.8	87 @ 10	35.2	5
MFN-MOFs/NF	1.0 M KOH	235 @ 50	55.4	79 @ 10	30.1	6
NiFe-NCs/CFP	1.0 M KOH	271 @ 10	48	197 @ 10	130	7
NiFe-MOF Array	0.1 M KOH	240 @ 10	34	134 @ 10	-	8
Fe1Ni4-HHTP NWs	1.0 M KOH	213 @ 10 300 @ 150	96	-	-	9
NiFe-NFF	1.0 M KOH	227 @ 10 253 @ 100	38.9	-	-	10
FN-2	1.0 M KOH	275 @ 10	56.7	-	-	11
(FeNi)-Tan/NF	1.0 M KOH	208 @ 50 223 @ 100	33.5	-	-	12
Ni-MOF@Fe-MOF	1.0 M KOH	265 @ 10	82	-	-	13
NiFe MOF/OM-NFH	1.0 M KOH	270 @ 10	123	-	-	14
Ni-Fe-MOF NSs	1.0 M KOH	221 @ 10 299 @ 100	56.0	-	-	15
Fe1Ni2-BDC	1.0 M KOH	260 @ 10	35	-	-	16
NiFex/NiFe2O4@NC	1.0 M KOH	262 @ 10	51.4	-	-	17
MIL-53(FeNi)/NF	1.0 M KOH	233 @ 50 244 @ 100	31.3	-	-	18
7.5-1h LDH-MOF@NF	1.0 M KOH	275.38 @ 10	47	-	-	19
NiFe-UMNs, hcp-NiFe@NC	1.0 M KOH	260 @ 10 226 @ 10	30 41	-	-	20 21
NiIIFeIII@NC	1.0 M KOH 0.1 M KOH	258 @ 10 360 @ 10	60 81	-	-	22
Ni0.75Fe0.25 BDC	0.1 M KOH	310 @ 10	43.7	-	-	23
ECD Fe/Ni-BTC@NF	0.1 M KOH	270 @ 10	47	-	-	24
4.3%-MOFs	0.1 M KOH	210 @ 200	68	-	-	25
NiFe-BDC(NH ₂) SURMOFD	0.1 M KOH	210 @ 200	26	-	-	26
NNU-23	0.1 M KOH	365 @ 10	77.2	-	-	27

Table S4 EIS fitting results of MOF electrocatalysts for OER and HER, respectively.

	Ni ₂ (dobpdc)	Ni ₂ (dobdc)	NiFe(dobpdc)	NiFe (dobdc)	Fe ₂ (dobpdc)	Fe ₂ (dobdc)
R _{ct} ^{a)}	39.7	73.0	5.4	13.1	19.6	36.5
R _{ct} ^{b)}	36.8	44.1	10.9	19.1	28.4	29.5

The R_{ct} values are for OER^{a)} and HER^{b)}, respectively.

Table S5 Predicted Bader charge (+e) of Fe atom in MOFs active sites for OER.

Models	*	HO*	O*	OOH*
NiFe(dobdc)	1.21	1.72	1.64	1.73
NiFe(dobpdc)	1.42	1.23	1.44	1.68

Table S6 Predicted Bader charge (+e) of Ni atom in MOFs active sites for OER.

Models	*	HO*	O*	OOH*
NiFe(dobdc)	1.23	1.20	1.18	1.19
NiFe(dobpdc)	1.27	1.24	1.21	1.04

Table S7 Predicted Gibbs free energy profiles of NiFe(dobdc) and NiFe(dobpdc) for OER, respectively.

Species	E (eV)	TS (eV) 298.15K	ZPE (eV)	CvT (eV)	G (eV)
O ₂ (g)	-9.86	0.63	0.10	0.049	-10.34
H ₂ (g)	-6.76	0.40	0.44	0.037	-6.69
H ₂ O(l)	-14.24	0.22	0.59	0.06	-13.81
NiFe(dobdc)					
NiFe(dobdc) + H ₂ O(l)	-2382.78				-1144.06
H ₂ O*	-2397.60	0.19	0.74	0.11	-2396.94
OH*	-2393.53	0.17	0.40	0.094	-2393.21
O*	-2387.39	0.16	0.11	0.083	-2387.36
OOH*	-2397.56	0.21	0.49	0.11	-2397.17
NiFe(dobdc) + O ₂ (g)	-2382.78				-1163.39
NiFe(dobpdc)					
NiFe(dobpdc) + H ₂ O(l)	-1213.23				-1144.06
H ₂ O*	-1228.14	0.18	0.71	0.10	-1227.51
OH*	-1223.65	0.20	0.38	0.11	-1223.37
O*	-1217.96	0.13	0.12	0.075	-1217.89
OOH*	-1227.88	0.23	0.48	0.12	-1227.51
NiFe(dobpdc) + O ₂ (g)	-1213.23				-1163.39

References

- 1 L. Sun, C. H. Hendon, S. S. Park, Y. Tulchinsky, R. Wan, F. Wang, A. Walsh and M. Dincă, *Chem. Sci.*, 2017, **8**, 4450-4457.
- 2 L. S. Xie, G. Skorupskii and M. Dincă, *Chem. Rev.*, 2020, **120**, 8536-8580.
- 3 X. Zhao, P. Pachfule, S. Li, J. R. J. Simke, J. Schmidt and A. Thomas, *Angew. Chem. Int. Ed.*, 2018, **57**, 8921-8926.
- 4 H.-W. Lin, D. Senthil Raja, X.-F. Chuah, C.-T. Hsieh, Y.-A. Chen and S.-Y. Lu, *Appl. Catal. B-Environ.*, 2019, **258**, 118023.
- 5 D. Senthil Raja, X.-F. Chuah and S.-Y. Lu, *Adv. Energy Mater.*, 2018, **8**, 1801065.
- 6 D. Senthil Raja, H.-W. Lin and S.-Y. Lu, *Nano Energy*, 2019, **57**, 1-13.
- 7 A. Kumar and S. Bhattacharyya, *ACS Appl. Mater. Interfaces*, 2017, **9**, 41906-41915.
- 8 J. Duan, S. Chen and C. Zhao, *Nat. Commun.*, 2017, **8**, 15341.
- 9 W.-H. Li, J. Lv, Q. Li, J. Xie, N. Ogiwara, Y. Huang, H. Jiang, H. Kitagawa, G. Xu and Y. Wang, *J. Mater. Chem. A*, 2019, **7**, 10431-10438.
- 10 C. Cao, D.-D. Ma, Q. Xu, X.-T. Wu and Q.-L. Zhu, *Adv. Funct. Mater.*, 2019, **29**, 1807418.
- 11 M. Liu, L. Kong, X. Wang, J. He and X.-H. Bu, *Small*, 2019, **15**, 1903410.
- 12 C. Li, G. Wang, K. Li, Y. Liu, B. Yuan and Y. Lin, *ACS Appl. Mater. Interfaces*, 2019, **11**, 20778-20787.
- 13 K. Rui, G. Zhao, Y. Chen, Y. Lin, Q. Zhou, J. Chen, J. Zhu, W. Sun, W. Huang and S. X. Dou, *Adv. Funct. Mater.*, 2018, **28**, 1801554.
- 14 X. Li, D.-D. Ma, C. Cao, R. Zou, Q. Xu, X.-T. Wu and Q.-L. Zhu, *Small*, 2019, **15**, 1902218.
- 15 F.-L. Li, P. Wang, X. Huang, D. J. Young, H.-F. Wang, P. Braunstein and J.-P. Lang, *Angew. Chem. Int. Ed.*, 2019, **58**, 7051-7056.
- 16 J. Li, W. Huang, M. Wang, S. Xi, J. Meng, K. Zhao, J. Jin, W. Xu, Z. Wang, X. Liu, Q. Chen, L. Xu, X. Liao, Y. Jiang, K. A. Owusu, B. Jiang, C. Chen, D. Fan, L. Zhou and L. Mai, *ACS Energy Lett.*, 2019, **4**, 285-292.
- 17 J. Zhao, X. Zhang, M. Liu, Y.-Z. Jiang, M. Wang, Z.-Y. Li and Z. Zhou, *J. Mater. Chem. A*, 2019, **7**, 21338-21348.
- 18 F. Sun, G. Wang, Y. Ding, C. Wang, B. Yuan and Y. Lin, *Adv. Energy Mater.*, 2018, **8**, 1800584.
- 19 J. Chen, P. Zhuang, Y. Ge, H. Chu, L. Yao, Y. Cao, Z. Wang, M. O. L. Chee, P. Dong, J. Shen, M. Ye and P. M. Ajayan, *Adv. Funct. Mater.*, 2019, **29**, 1903875.
- 20 G. Hai, X. Jia, K. Zhang, X. Liu, Z. Wu and G. Wang, *Nano Energy*, 2018, **44**, 345-352.
- 21 C. Wang, H. Yang, Y. Zhang and Q. Wang, *Angew. Chem. Int. Ed.*, 2019, **58**, 6099-6103.
- 22 L. Du, L. Luo, Z. Feng, M. Engelhard, X. Xie, B. Han, J. Sun, J. Zhang, G. Yin, C. Wang, Y. Wang and Y. Shao, *Nano Energy*, 2017, **39**, 245-252.
- 23 Y. Hao, Q. Liu, Y. Zhou, Z. Yuan, Y. Fan, Z. Ke, C.-Y. Su and G. Li, *Energy Environ. Mater.*, 2019, **2**, 18-21.
- 24 L. Wang, Y. Wu, R. Cao, L. Ren, M. Chen, X. Feng, J. Zhou and B. Wang, *ACS Appl. Mater. Interfaces*, 2016, **8**, 16736-16743.
- 25 W. Cheng, X. Zhao, H. Su, F. Tang, W. Che, H. Zhang and Q. Liu, *Nat. Energy*, 2019, **4**, 115-122.
- 26 W. Li, S. Xue, S. Watzele, S. Hou, J. Fichtner, A. L. Semrau, L. Zhou, A. Welle, A. S. Bandarenka and R. A. Fischer, *Angew. Chem. Int. Ed.*, 2020, **59**, 5837-5843.
- 27 X.-L. Wang, L.-Z. Dong, M. Qiao, Y.-J. Tang, J. Liu, Y. Li, S.-L. Li, J.-X. Su and Y.-Q. Lan, *Angew. Chem. Int. Ed.*, 2018, **57**, 9660-9664.